Laboratory-frame electron angular distributions: Probing the chemical environment through intramolecular electron scattering

M. Patanen,[1] O. Travnikova,[1] M. G. Zahl,[2] J. Söderström,[3] P. Decleva,[4] T. D. Thomas,[5] S. Svensson,[3] N. Mårtensson,[3] K. J. Børve,[2] L. J. Sæthre,[2] and C. Miron[1,*]

[1]*Synchrotron SOLEIL, L'Orme des Merisiers, Saint-Aubin, BP 48, 91192 Gif-sur-Yvette Cedex, France*
[2]*Department of Chemistry, University of Bergen, Allégaten 41, 5007 Bergen, Norway*
[3]*Department of Physics and Astronomy, Uppsala University, Box 516, 75120 Uppsala, Sweden*
[4]*Department of Chemical and Pharmaceutical Sciences, University of Trieste, Via L. Giorgieri 1, 34127 Trieste, Italy*
[5]*Department of Chemistry, Oregon State University, Corvallis, Oregon 97331-4003, USA*
(Received 24 November 2012; revised manuscript received 21 May 2013; published 21 June 2013)

Carbon 1s photoelectron asymmetry parameters β for the chlorinated and the methyl carbon atom of CH_3CH_2Cl, CH_3CHCl_2, and CH_3CCl_3 have been measured using synchrotron radiation in the 340–600 eV energy range. We provide experimental evidence that the intramolecular scattering strongly affects β values, even far from the ionization threshold. The results are in agreement with B-spline density functional theory calculations, making it possible to single out the behavior of the various continuum partial waves. We conclude that the intramolecular scattering makes electron angular distributions sensitive to the chemical environment, even in isolated gas phase molecules.

I. INTRODUCTION

Photoelectron diffraction and angularly resolved photoemission have been useful tools to study adsorbates on surfaces for over 30 years [1–3]. Concerning the essentially randomly oriented gas phase molecules, multicoincidence techniques make it possible to select an oriented ensemble of molecules with respect to the polarization vector of the light, and measure the molecular frame photoelectron angular distributions (MFPADs) [4,5]. As suggested by Dill *et al.* in 1976 [6], they have a rich structure inherently including information about the photoionization dynamics. MFPADs are affected by photoelectron diffraction phenomena, thus providing a way to access information related to the molecular potentials and to determine the internuclear distances in gas phase diatomic molecules, for instance [7–10]. The technique above relies on the axial recoil approximation, assuming dissociation processes significantly faster than molecular rotation. The methodology becomes more challenging for polyatomic molecules, where a two-body dissociation channel has to be identified to make it applicable for the selection of the molecular frame.

Very recently, photoelectron diffraction was experimentally and theoretically identified in the vibrationally resolved C 1s photoionization cross-section ratios of randomly oriented gas phase CH_4 molecules [11], allowing to extract the C–H bond length from the modeling of the noncoincident, nonangularly resolved photoelectron spectroscopy measurements. Furthermore, a study by Söderström *et al.* [12] revealed the existence of oscillations in the C 1s photoionization cross-section ratios of two inequivalent C atoms in gas phase chloroethane (CH_3CH_2Cl), 1,1-dichloroethane (CH_3CHCl_2), and 1,1,1-trichloroethane (CH_3CCl_3) as a function of photon energy. The measured ratios were far from the stoichiometric

expectations, and the oscillatory behavior was shown to persist up to several hundred eVs above the photoionization thresholds. The observed oscillations of the intensity ratios were enhanced when more H atoms were replaced by Cl atoms, and they were interpreted as extended x-ray absorption fine structure (EXAFS) -type modulations mainly due to the scattering from the Cl atoms. Compared to the EXAFS oscillations observed in electron energy loss spectra of gas phase molecules a long time ago [13–15], the photoionization method benefits from the chemical selectivity associated with the chemical shifts of the core levels and, as will be shown in this paper, provides a possibility to study the angular dependence of the cross sections for each "chemically shifted" atom of the same element.

A computational study of the nonstoichiometric behavior of C 1s cross sections in different hydrocarbons has been carried out by Di Tommaso and Decleva [16]. They predicted a strong oscillatory behavior in the intensity ratios: (i) sharp structures close to the ionization thresholds due to shape resonances, and (ii) smoother, nonvanishing oscillations at higher energies due to the scattering from neighboring atoms. Even earlier, Natalense *et al.* [17] compared the angular dependence of the C 1s photoionization cross sections in CH_4, CF_4, and CCl_4, close to threshold. They pointed out that the complete replacement of H by F and Cl remarkably modifies the C 1s cross sections and asymmetry parameters. While shape resonances [18] were known to affect the angular distributions of photoelectrons [19], more recently vibrationally specific cross sections and photoelectron angular distributions have been shown to strongly deviate from the Franck-Condon behavior close to the photoionization thresholds (see, e.g., [20,21] and references therein).

In this paper, the angularly resolved C 1s photoelectron spectra and asymmetry parameters β for two inequivalent carbon atoms in CH_3CH_2Cl, CH_3CHCl_2, and CH_3CCl_3 are discussed. The measurements were performed with photon energies 340, 360, 400, and 600 eV to avoid the vicinity

_____

*Author to whom all correspondence should be addressed: Catalin.Miron@synchrotron-soleil.fr

of shape resonances. We observe a strong x-ray polarization dependence in intensity ratios of the chlorinated (CH_xCl_{3-x}, $x = 0, 1, 2$) versus the methyl group (CH_3) C 1s lines, reflected in the β parameters, which exhibit a high sensitivity to the chemical environment of the emitter.

II. EXPERIMENT

The experiment was carried out at the PLEIADES beamline [22–25] at the SOLEIL national synchrotron radiation facility in Saint-Aubin, France. The Apple II permanent magnet HU80 (80 mm period) undulator was used to provide linearly polarized light with $0°$, $90°$, and $54.7°$ between the polarization vector and the electron detection axis. The C 1s photolines were recorded using a $30°$ wide angle lens VG-Scienta R4000 electron energy analyzer installed on the C-branch of the beamline [23].

CH_3CCl_3 and CH_3CHCl_2 are liquids (99.998% purity from Sigma Aldrich) at room temperature, and before introducing their vapors into a differentially pumped gas cell, the dissolved air was removed using freeze-pump-thaw cycles. CH_3CH_2Cl, 99.7% pure gas from Sigma Aldrich was used without further purification. The gas cell is equipped with a series of electrodes used to minimize the local effect of plasma potentials caused by the ion density gradient created along the synchrotron radiation propagation axis. The gas pressure was about 4×10^{-6} mbar in the spectrometer chamber, and approximately two to three orders of magnitude higher in the interaction region inside the gas cell. At these pressures, the mean free path of the molecules is 0.1–1 m, making the effect of the pressure negligible.

For the measurements of the CH_3CCl_3 and CH_3CHCl_2 spectra, a monochromator exit slit of 115 μm and a varied groove depth (VGD) plane grating with 1600 grooves/mm were used. A pass energy of 100 eV and a curved entrance slit of 0.8 mm were used for the electron energy analyzer. These settings provide approximate electron energy resolutions of 206, 208, 210, and 232 meV for the photolines measured at the photon energies 340, 360, 400, and 600 eV, respectively. For CH_3CH_2Cl, a VGD grating with 2400 grooves/mm was used with an exit slit of 125 μm. The pass energy of the electron analyzer was 50 eV and the same 0.8 mm curved entrance slit was used. Thus, the estimated electron energy resolution was 110, 112, 116, and 145 meV for the photolines measured at the same photon energies as above. In the estimation of the resolution, the only Doppler effect taken into account was the translational Doppler broadening, being easier to estimate, even though under the present conditions it is very small compared to the instrumental broadening caused by the electron analyzer itself, and approximately the same for all samples (7–27 meV). Spectra were normalized with respect to sample pressure, acquisition duration, and photon flux, which was continuously monitored by a photodiode, in order to obtain comparable intensities between different measurements.

III. DATA ANALYSIS

C 1s photolines were fitted using Igor Pro software by WaveMetrics, Inc. and the SPANCF fitting macros by Kukk [26]. To be able to properly account for the complex vibrational structure of the two C 1s photoionization peaks presented for
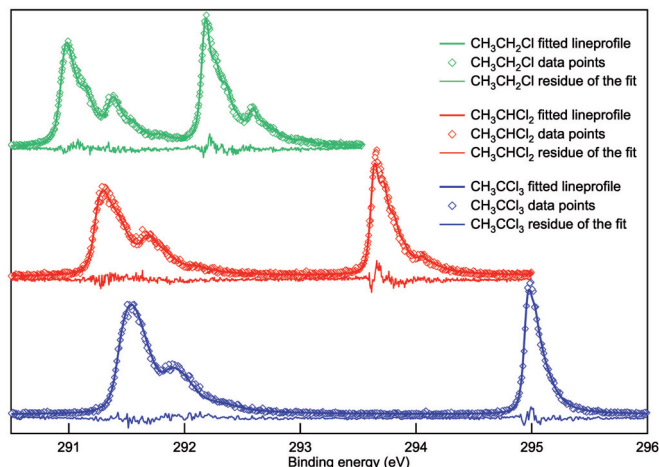

FIG. 1. (Color online) High-resolution C 1s photoelectron spectra of CH_3CH_2Cl (green), CH_3CHCl_2 (red), and CH_3CCl_3 (blue) measured with 340 eV photons at $54.7°$ with respect to the light polarization vector, with approximately 38 meV of instrumental broadening. Experimental data points are presented as diamonds, thick solid lines present the fitted calculated line profiles, and thin solid lines show the residual of the fit.

each molecule in Fig. 1, the vibrational transitions calculated within the Franck-Condon approximation (see Sec. IV A for a detailed discussion of the line-shape calculations) were fitted to the experimental data as described below. Post-collisional interaction (PCI) line shapes were used in the fitting process. A recent study by Zahl *et al.* [27] showed that chemical substitution has a strong effect on the lifetimes of core-ionized states, as suggested earlier by Thomas *et al.* [28] for a different series of compounds. Therefore, the Lorentzian widths were optimized separately for the two inequivalent carbons in the compound, whereas they were constrained to be the same for all spectra measured with different photon energies and polarizations. The Gaussian width accounting for the instrumental and translational Doppler broadening was forced to have the same value for all peaks for a given photon energy.

The experimental asymmetry parameters β were extracted for both chlorinated and methyl group carbons using data from the $0°$ and $90°$ measurements. This method requires a careful normalization of the experimental spectra in order to obtain the intensities $I_{0°}$ and $I_{90°}$ (areas of the C 1s photolines) independent of photon flux, gas pressure, or data collection time. To obtain β, the following formula was used:

$$\beta = 2[I_{0°}/I_{90°} - 1]/[I_{0°}/I_{90°} + 2], \tag{1}$$

where I_θ is the intensity measured at the indicated angle. An alternate method described by Kivimäki *et al.* [29] uses $0°$ and $90°$ together with measurements performed at the so-called "magic angle," $54.7°$, where the photoionization cross section is independent of β. With this method there is no need for normalization to account for the experimental conditions. We have also used this method to calculate the values of β, which are in agreement with those obtained by the method described above. However, the uncertainties obtained by the latter method are large if β_{CH} and β_{CCl} are nearly equal (as in our case at high photon energies). Therefore, these results are not shown.

The error bars for β were defined using the differential

$$\Delta \beta = \frac{\partial \beta}{\partial R'} \Delta R' = \frac{6}{(R'+2)^2} \Delta R',$$

$$R' = \frac{I_{0^\circ}}{I_{90^\circ}}, \tag{2}$$

$$\Delta R' = \sqrt{\left[\frac{\Delta I_{0^\circ}}{I_{90^\circ}}\right]^2 + \left[\frac{I_{0^\circ} \Delta I_{90^\circ}}{I_{90^\circ}^2}\right]^2}.$$

ΔI_{90° and ΔI_{0° were estimated using the error analysis tools available in the SPANCF fitting package [26]. It can be shown that the error in β can be evaluated using the error in the ratios R' calculated as an intermediate result, giving the same result as when taking the differential with respect to I_{0° and I_{90° directly.

In the error analysis, the possible error in the computed line shapes was not taken into account. When trying different fitting schemes with different sets of free parameters (e.g., Lorentzian broadenings fixed, Gaussian broadening free), it was noticed that the changes in the actual β parameters were small, since the calculated line shapes describe the area of the photolines very well in all schemes.

IV. CALCULATIONS

A. Calculations of the C 1s photoionization line shapes

Geometries for the ground and ionized states, normal modes, and harmonic frequencies of the studied chloroethanes were calculated at the MP4SDQ level of theory using the GAUSSIAN09 (G09) package of programs [30]. Cl was represented using the basis set of McLean and Chandler [31] augmented with a double polarization set prepared from the original single d exponent $\alpha = 0.75$ by replacing it by $2\alpha = 1.50$ and $\alpha/2 = 0.375$ [32,33]. C and H where represented using a Dunning triple-ζ basis plus polarization functions [34,35]. For the ionized C, the corresponding N basis was used, with all exponents scaled by a factor 0.9293 [36]. The core of the ionized C was represented using the effective core potential of Stevens *et al.* [37] scaled to account for only one electron in the 1s shell [38]. The ASYM program [39] was used to express normal coordinates in internal coordinates. Franck-Condon factors were computed by the algorithm of Ansbacher [40] and by using the parallel-modes approach, i.e., mode-mixing is neglected while differences in vibrational frequencies between the neutral and ionized states are accounted for. (For more information, see the Appendix in Ref. [41].) The harmonic approximation was applied for all modes except for the symmetric C–H stretching mode of the ionized C, which was described by a Morse potential. The contraction of the C–H bond of the ionized C was reduced by 0.30 pm to account for core-valence correlation and basis-set incompleteness errors [38]. Correspondingly, the contraction of the C–Cl bond of the ionized C was reduced by 0.40 pm [27]. Frequencies were scaled by a general scaling factor of 0.99. In addition, the symmetric C–H stretching frequency of the ionized C was scaled by 0.97 [36].

Line-shape calculations omitted the effect of the vibrational intensity redistribution caused by intramolecular scattering [11], so the same line shape was used for all the photon energies and light polarizations. Recoil effects were not taken into account [42,43]. Due to the moderate resolution used in the 90° and 0° measurements, no visible effect was seen in the fits that would have indicated significant distortion of the modeled line shape. In the present case, only the relative intensities of the full photoelectron peaks are of interest, and thus as far as the modeled line shape fits the whole photoelectron peak structure well, small intensity changes between vibrational modes within a peak are less important. The studied samples have eight atoms in a molecule, so these effects are very difficult to resolve experimentally due to the large number of degrees of freedom and thus the large amount of vibrational levels excited.

B. Calculations of the C 1s cross sections

To model the role of the intramolecular scattering on the laboratory-frame electron angular distribution, the photoionization observables (cross sections and asymmetry parameters) have been computed employing a density functional theory (DFT) approach. The one-particle Kohn-Sham Hamiltonian h_{KS} is completely defined by the ground-state density. Bound and continuum eigenvectors have been obtained in a basis of multicentric B-spline functions, which effectively takes into account the Coulomb singularities at the nuclei and affords a convergent solution also for complex polyatomic molecules and deep core holes [44,45]. Fixed nuclei calculations have been performed at the equilibrium geometries previously obtained. The initial ground-state densities have been obtained by a conventional DFT calculation employing the ADF program [46], with a double-zeta polarized (DZP) basis from the ADF database, and the LB94 exchange-correlation potential [47], which has also been employed in the following continuum calculations. Cross sections and asymmetry parameters have been obtained from standard angular momentum analysis [48]. The maximum angular momentum in the one-center part of the B-spline calculation is $l_{max} = 20$, which ensures convergence up to about 570 eV electron kinetic energy. Convergence has been also verified for CH_3CCl_3 by employing $l_{max} = 24$.

V. RESULTS AND DISCUSSION

Figure 2 presents the C 1s photoelectron spectra recorded with 340 eV photon energy with 0° and 90° polarizations. The K-shell ionization of the chlorinated C leads to a photoline of higher binding energy as compared to the methyl C 1s photoline. As already reported in Ref. [12] for 54.7° polarization, the intensity ratios of chlorinated and methyl C 1s photolines vary as a function of photon energy due to intramolecular scattering. Now the effect of scattering is clearly evidenced at a given photon energy but between two different polarizations. For example, if we compare the CH_3CCl_3 spectra measured at 340 eV [Fig. 2(c)], it is seen that the photoline of chlorinated C is obviously enhanced at 90° as compared to the methyl C photoline. The same holds for CH_3CHCl_2 and CH_3CH_2Cl, as well as for different photon energies, the enhancement being gradually less pronounced when the degree of Cl substitution decreases.

Let us introduce a simple physical picture describing the effect of scattering on the electron angular distributions for
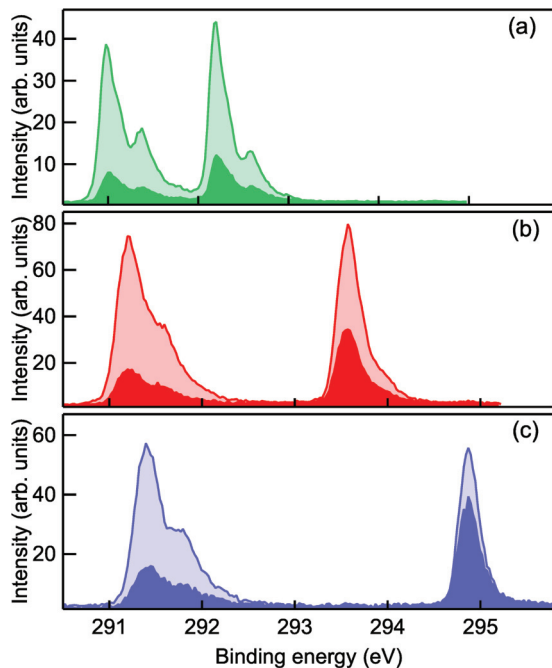
FIG. 2. (Color online) C $1s$ photoelectron spectra of (a) CH_3CH_2Cl, (b) CH_3CHCl_2, and (c) CH_3CCl_3 measured with $0°$ (light) and $90°$ (dark) polarizations and 340 eV photon energy. The spectra are normalized with respect to acquisition duration, photon flux, and gas pressure. All spectra acquired at $90°$ are multiplied by a factor of 3 for easier visual comparison.
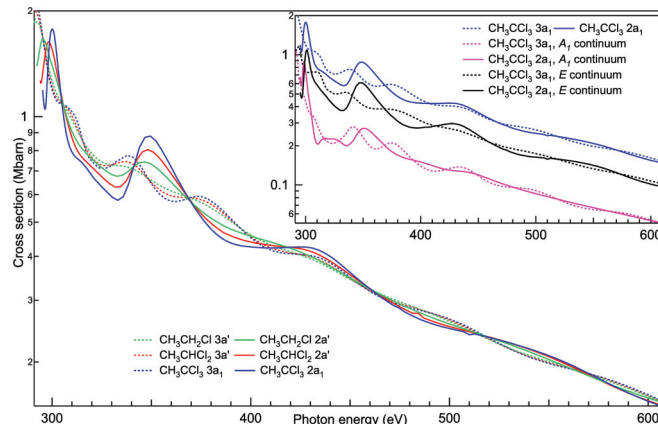

FIG. 3. (Color online) Theoretical C $1s$ photoionization cross sections corresponding to the ionization of the chlorinated (solid lines) and the methyl carbon (dashed lines) of CH_3CH_2Cl (green), CH_3CHCl_2 (red), and CH_3CCl_3 (blue). The pink and black solid and dotted lines in the inset show the contributions of A_1 and E continuum channels in the case of CH_3CCl_3 (see text for details).

different polarizations and ionization continua. CH_3CCl_3 is discussed as an example, but the discussion is also applicable to CH_3CH_2Cl and CH_3CHCl_2. The C $1s$ orbitals in CH_3CCl_3 (C_{3v} symmetry) are $2a_1$ (chlorinated C) and $3a_1$ (methyl C) (the corresponding orbitals are $2a'$ and $3a'$ in CH_3CH_2Cl and CH_3CHCl_2, both of C_s symmetry). The ionization of an a_1 orbital leads to a continuum wave of A_1 or E symmetry.

In the dipole approximation, the E continuum will preferentially "select" the molecules with their molecular axis perpendicular to the polarization vector **e**, and thus parallel (perpendicular) to the electron detection axis for the $90°$ ($0°$) scheme. The crude central potential model approximation leads for C $1s$ photoionization to the ideal energy-independent $\beta = 2$ parameter [49], the electrons being emitted with a $\cos^2 \theta$ distribution, θ being the angle between the photoelectron momentum and the **e** vector. When **e** is perpendicular to the detection axis, no signal should be detected, and when **e** and the detection axis are parallel, the maximum signal should be detected. However, this is not the case experimentally. In addition to the well-known relativistic or nonrelativistic (anisotropic) electron-ion or configuration interactions extensively discussed for atoms [49,50], the origin of the present observation is a molecular effect. The emitted electrons are scattered by the surrounding atoms, which affects their angular distribution and allows some of them to reach the detector in a $90°$ scheme, lowering the signal at $0°$. In the present case, since the scattering cross section is smaller for H than for Cl, the relative signal from the chlorinated C is larger than from the methyl C at $90°$ (Fig. 2). Correspondingly, a decrease of the electron signal in the $0°$ detection scheme is observed. In the

case of the A_1 continuum, the molecules with the molecular axis parallel to the **e** will be preferentially "selected" and a discussion analogous to the above leads to similar conclusions.

Figure 3 illustrates the photoionization cross sections of the chlorinated C $1s$ ($2a_1$ and $2a'$) and methyl C $1s$ ($3a_1$ and $3a'$) orbitals for CH_3CH_2Cl, CH_3CHCl_2, and CH_3CCl_3. All cross sections show similar oscillatory behavior, but the amplitude of the oscillations is the largest for CH_3CCl_3 and the smallest for CH_3CH_2Cl. A surprisingly sharp first peak, seen in the $2a_1$ and $2a'$ cross sections, is assigned to a shape resonance, whereas in the $3a_1$ and $3a'$ cross sections a smooth oscillatory behavior is observed already at the lowest photon energies. The second clear peak observed in the $2a_1$ and $2a'$ cross sections is located too high in energy (~ 60 eV above threshold) to be assigned to a shape resonance, and it is interpreted to be the first unambiguous fingerprint of intramolecular scattering. Contrary to the cross-section oscillations typical of the coherent emission from equivalent centers [51], the oscillatory structures of the chlorinated and methyl C $1s$ cross sections are not in phase opposition. In the $2a_1$ and $2a'$ channels, the oscillations have significantly longer periods and larger amplitudes compared to the $3a_1$ and $3a'$ channels, which exhibit more regular and less damped structures.

The inset in Fig. 3 shows the partial E and A_1 continua contributions to the $2a_1$ and $3a_1$ photoionization cross sections of CH_3CCl_3. For $2a_1$, the largest contribution comes from the E channel due to its twofold degeneracy; the A_1 channel shows a modest contribution to the sharp peak around 350 eV, and then it is mostly flat. Interestingly, it also shows a lower energy structure before 350 eV, which is, however, hidden by background in the total cross section. For $3a_1$, both A_1 and E channels show important oscillations, generally not in phase, and therefore the oscillations in the total cross section come from the superposition of the two different contributions. The lowest energy oscillations are associated with the E channel. Oscillations in the A_1 channel persist even at high energies, whereas in the E channel they are more strongly damped.
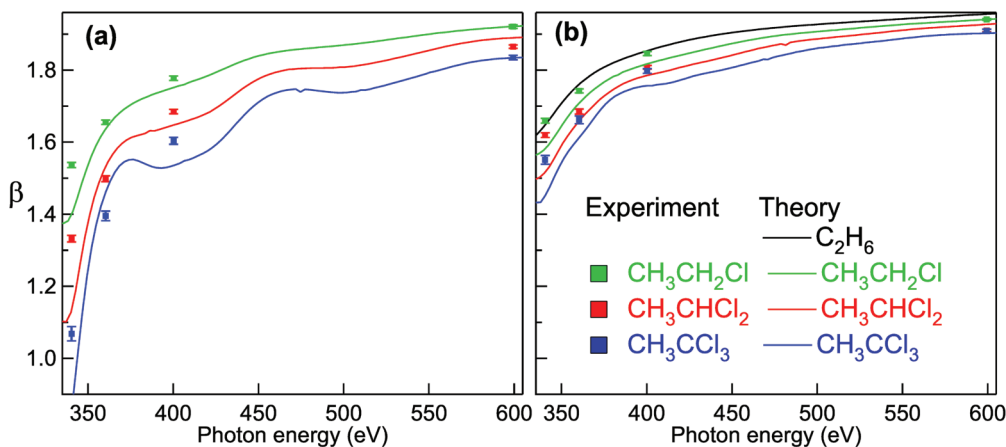
FIG. 4. (Color online) Photoelectron asymmetry parameters in CH_3CH_2Cl, CH_3CHCl_2, and CH_3CCl_3 of (a) chlorinated and (b) methyl C $1s$.

Based on the above analysis, we assign the features observed in the A_1 channel mostly to electron diffraction by the neighboring C atom, as it corresponds to photoelectrons essentially ejected along the C–C bond. The E component is mostly sensitive to the surrounding Cl atoms (the H atoms having a minor effect), since the photoelectron escapes mainly in the perpendicular direction. This explains the larger amplitude of the oscillations and the longer period in the $2a_1 - E$ channel as compared to $3a_1$ (shorter C-Cl distance). A much smaller effect is seen in the A_1 component of the $2a_1$ cross section. However, the lowest energy feature could be a signature of the diffraction by the other C atom. In contrast, the electron ejected from the $3a_1$ orbital is diffracted with similar intensity by both the other C and the Cl atoms (note that the Cl group has also an a_1 component, contributing to the scattering of the a_1 continuum wave), so both A_1 and E components have similar oscillation amplitudes.

Figure 4 presents the theoretical and the experimental β values for C $1s$ photoionization in CH_3CH_2Cl, CH_3CHCl_2, and CH_3CCl_3. In addition, the theoretical β parameter for C $1s$ photoionization of ethane C_2H_6, an average β from the $1a_{1g}$ and $1a_{2u}$ ionization cross sections, has been plotted together with the methyl group β, offering a "Cl-free" reference. The asymmetry parameters for the chlorinated carbon show a clear trend, with CH_3CCl_3 showing the largest β-variation in the considered energy range. The changes in the methyl C β values are much smaller. A similar trend can be seen in the computational study by Di Tommaso and Decleva [16] in the C $1s$ β parameters of fluoroacetylene (FCCH) and 1,1-difluoroethene (F_2CCH_2). The asymmetry parameter is lower for the fluorinated C and, in FCCH, approaches faster the β value for the nonfluorinated C than in F_2CCH_2. In our case, the effect of the substitution is particularly marked in the low-energy region, where a large, steep decrease toward threshold is observed for the C $1s$ β parameter of the substituted carbon. A somewhat weaker but consistent effect is also observed for the C $1s$ β of the methyl group, which gradually approaches the β of ethane when the degree of Cl substitution is decreased. Theoretical and experimental data are in generally good agreement, although the calculated values are systematically lower than the experimental ones.

At higher energies, the methyl C β shows a monotonic increase, while the β parameters of the substituted carbon show noticeable oscillations in the calculated profiles, which become increasingly marked with increasing substitution. The oscillation period is close to that observed in the cross sections, so one can assign it to the same origin, the photoelectron diffraction. Unfortunately, the experimental values are too sparse to reproduce this oscillatory effect. Even at the highest energy considered, the β parameters of the substituted carbon remain lower than those of the methyl carbon, and the β values follow the order $CCl_3 < CHCl_2 < CH_2Cl < CH_3$, as can be seen in Fig. 4.

VI. CONCLUSIONS

In conclusion, using experimental and theoretical analysis, we have pointed out a pure molecular effect by demonstrating the importance of intramolecular scattering on the photoelectrons' angular distributions. We have shown that chemical substitution has a large effect on the β parameters. In particular, at the low photon energies the photoelectrons emitted from the substituted carbon are efficiently redirected from their trajectories by the scattering from the surrounding Cl atoms. The scattering effect is also observed in the β parameters of the methyl group carbon, showing smaller but consistent modulations: the more halogenated the molecule is, the more β parameters deviate from their asymptotic values. The observations are supported by theoretical calculations, making it possible to single out the various continuum channel contributions. The angularly resolved photoelectron spectroscopy in the laboratory frame is found to be sensitive to the chemical environment, depending on intramolecular scattering effects even in randomly oriented molecules.

[1] D. P. Woodruff, D. Norman, B. W. Holland, N. V. Smith, H. H. Farrell, and M. M. Traum, Phys. Rev. Lett. **41**, 1130 (1978).

[2] A. Liebsch, Phys. Rev. Lett. **32**, 1203 (1974).

[3] D. P. Woodruff, J. Electron Spectrosc. Relat. Phenom. **100**, 259 (1999).

[4] A. V. Golovin, N. A. Cherepkov, and V. V. Kuznetsov, Z. Phys. D **24**, 371 (1992).

[5] E. Shigemasa, J. Adachi, M. Oura, and A. Yagishita, Phys. Rev. Lett. **74**, 359 (1995).

[6] D. Dill, J. Siegel, and J. L. Dehmer, J. Chem. Phys. **65**, 3158 (1976).

[7] A. L. Landers, Th. Weber, I. Ali, A. Cassimi, M. Hattass, O. Jagutzki, A. Nauert, T. Osipov, A. Staudte, M. H. Prior, H. Schmidt-Böcking, C. L. Cocke, and R. Dörner, Phys. Rev. Lett. **87**, 013002 (2001).

[8] S. E. Canton, E. Plésiat, J. D. Bozek, B. S. Rude, P. Decleva, and F. Martín, Proc. Natl. Acad. Sci. (USA) **108**, 7302 (2011).

[9] X.-J. Liu, N. A. Cherepkov, S. K. Semenov, V. Kimberg, F. Gel'mukhanov, G. Prümper, T. Lischke, T. Tanaka, M. Hoshino, H. Tanaka, and K. Ueda, J. Phys. B **39**, 4801 (2006).

[10] B. Zimmermann *et al.*, Nat. Phys. **4**, 649 (2008).

[11] E. Plésiat, L. Argenti, E. Kukk, C. Miron, K. Ueda, P. Decleva, and F. Martín, Phys. Rev. A **85**, 023409 (2012).

[12] J. Söderström, N. Mårtensson, O. Travnikova, M. Patanen, C. Miron, L. J. Sæthre, K. J. Børve, J. J. Rehr, J. J. Kas, F. D. Vila, T. D. Thomas, and S. Svensson, Phys. Rev. Lett. **108**, 193005 (2012).

[13] A. P. Hitchcock and C. E. Brion, J. Electron Spectrosc. Relat. Phenom. **14**, 417 (1978).

[14] B. X. Yang, J. Kirz, and T. K. Sham, Phys. Rev. A **36**, 4298 (1987).

[15] J. Stöhr and K. R. Bauchspiess, Phys. Rev. Lett. **67**, 3376 (1991).

[16] D. Di Tommaso and P. Decleva, J. Chem. Phys. **123**, 064311 (2005).

[17] A. P. P. Natalense, L. M. Brescansin, and R. R. Lucchese, Phys. Rev. A **68**, 032701 (2003).

[18] M. N. Piancastelli, J. Electron Spectrosc. Relat. Phenom. **100**, 167 (1999).

[19] C. M. Truesdale, S. H. Southworth, P. H. Kobrin, U. Becker, D. W. Lindle, H. G. Kerkhoff, and D. A. Shirley, Phys. Rev. Lett. **50**, 1265 (1983); D. Dill, J. R. Swanson, S. Wallace, and J. L. Dehmer, *ibid.* **45**, 1393 (1980).

[20] D. A. Mistrov, A. De Fanis, M. Kitajima, M. Hoshino, H. Shindo, T. Tanaka, Y. Tamenori, H. Tanaka, A. A. Pavlychev, and K. Ueda, Phys. Rev. A **68**, 022508 (2003).

[21] R. R. Lucchese, J. Söderström, T. Tanaka, M. Hoshino, M. Kitajima, H. Tanaka, A. De Fanis, J.-E. Rubensson, and K. Ueda, Phys. Rev. A **76**, 012506 (2007).

[22] O. Travnikova, J.-C. Liu, A. Lindblad, C. Nicolas, J. Söderström, V. Kimberg, F. Gel'mukhanov, and C. Miron, Phys. Rev. Lett. **105**, 233001 (2010).

[23] J. Söderström, A. Lindblad, A. Grum-Grzhimailo, O. Travnikova, C. Nicolas, S. Svensson, and C. Miron, New J. Phys. **13**, 073014 (2011).

[24] C. Miron, C. Nicolas, O. Travnikova, P. Morin, Y. P. Sun, F. Gelmukhanov, N. Kosugi, and V. Kimberg, Nat. Phys. **8**, 135 (2012).

[25] A. Lindblad, V. Kimberg, J. Söderström, C. Nicolas, O. Travnikova, N. Kosugi, F. Gel'mukhanov, and C. Miron, New J. Phys. **14**, 113018 (2012).

[26] E. Kukk, Spectrum Analysis by Curve Fitting (SPANCF) Macro Package for Igor Pro, http://www.physics.utu.fi/en/department/materials_research/materials_science/Fitting.html.

[27] M. G. Zahl, K. J. Børve, and L. J. Sæthre, J. Electron Spectrosc. Relat. Phenom. **185**, 226 (2012).

[28] T. D. Thomas, C. Miron, K. Wiesner, P. Morin, T. X. Carroll, and L. J. Sæthre, Phys. Rev. Lett. **89**, 223001 (2002).

[29] A. Kivimäki, E. Kukk, J. Karvonen, J. Mursu, E. Nõmmiste, H. Aksela, and S. Aksela, Phys. Rev. A **57**, 2724 (1998).

[30] GAUSSIAN 09, Revision B.01, M. J. Frisch, G. W. Trucks, H. B. Schlegel, G. E. Scuseria, M. A. Robb, J. R. Cheeseman, G. Scalmani, V. Barone, B. Mennucci, G. A. Petersson, H. Nakatsuji, M. Caricato, X. Li, H. P. Hratchian, A. F. Izmaylov, J. Bloino, G. Zheng, J. L. Sonnenberg, M. Hada, M. Ehara, K. Toyota, R. Fukuda, J. Hasegawa, M. Ishida, T. Nakajima, Y. Honda, O. Kitao, H. Nakai, T. Vreven, J. A. Montgomery, Jr., J. E. Peralta, F. Ogliaro, M. Bearpark, J. J. Heyd, E. Brothers, K. N. Kudin, V. N. Staroverov, R. Kobayashi, J. Normand, K. Raghavachari, A. Rendell, J. C. Burant, S. S. Iyengar, J. Tomasi, M. Cossi, N. Rega, J. M. Millam, M. Klene, J. E. Knox, J. B. Cross, V. Bakken, C. Adamo, J. Jaramillo, R. Gomperts, R. E. Stratmann, O. Yazyev, A. J. Austin, R. Cammi, C. Pomelli, J. W. Ochterski, R. L. Martin, K. Morokuma, V. G. Zakrzewski, G. A. Voth, P. Salvador, J. J. Dannenberg, S. Dapprich, A. D. Daniels, Ö. Farkas, J. B. Foresman, J. V. Ortiz, J. Cioslowski, and D. J. Fox, Gaussian, Inc., Wallingford, CT (2009).

[31] A. D. McLean and G. S. Chandler, J. Chem. Phys. **72**, 5639 (1980).

[32] M. M. Francl, W. J. Pietro, W. J. Hehre, J. S. Binkley, M. S. Gordon, D. J. DeFrees, and J. A. Pople, J. Chem. Phys. **77**, 3654 (1982).

[33] M. J. Frisch, J. A. Pople, and J. S. Binkley, J. Chem. Phys. **80**, 3265 (1984).

[34] T. H. Dunning, Jr., J. Chem. Phys. **55**, 716 (1971).

[35] R. Krishnan, J. S. Binkley, R. Seeger, and J. A. Pople, J. Chem. Phys. **72**, 650 (1980).

[36] T. Karlsen, K. J. Børve, L. J. Sæthre, K. Wiesner, M. Bässler, and S. Svensson, J. Am. Soc. Chem. **124**, 7866 (2002).

[37] W. J. Stevens, H. Basch, and M. Krauss, J. Chem. Phys. **81**, 6026 (1984).

[38] T. Karlsen and K. J. Børve, J. Chem. Phys. **112**, 7979 (2000).

[39] L. Hedberg and I. M. Mills, J. Molec. Spectrosc. **160**, 117 (1993).

[40] F. Ansbacher, Z. Naturforsch. A **14**, 889 (1959).
[41] V. M. Oltedal, K. J. Børve, L. J. Sæthre, T. D. Thomas, J. D. Bozek, and E. Kukk, Phys. Chem. Chem. Phys. **6**, 4254 (2004).
[42] E. Kukk, K. Ueda, U. Hergenhahn, X.-J. Liu, G. Prümper, H. Yoshida, Y. Tamenori, C. Makochekanwa, T. Tanaka, M. Kitajima, and H. Tanaka, Phys. Rev. Lett. **95**, 133001 (2005).
[43] E. Kukk, K. Ueda, and C. Miron, J. Electron Spectrosc. Relat. Phenom. **185**, 278 (2012).
[44] D. Toffoli, M. Stener, G. Fronzoni, and P. Decleva, Chem. Phys. **276**, 25 (2002).
[45] H. Bachau, E. Cormier, P. Decleva, J. E. Hansen, and F. Martín, Rep. Prog. Phys. **64**, 1815 (2001).

[46] C. Fonseca Guerra, J. G. Snijders, G. te Velde, and E. J. Baerends, Theor. Chem. Acc. **99**, 391 (1998).
[47] R. Van Leeuwen and E. J. Baerends, Phys. Rev. A **49**, 2421 (1994).
[48] N. Chandra, J. Phys. B **20**, 3405 (1987).
[49] S. T. Manson and A. F. Starace, Rev. Mod. Phys. **54**, 389 (1982).
[50] N. M. Kabachnik, S. Fritzsche, A. N. Grum-Grzhimailo, M. Meyer, and K. Ueda, Phys. Rep. **451**, 155 (2007).
[51] L. Argenti, T. D. Thomas, E. Plésiat, X. J. Liu, C. Miron, T. Lischke, G. Prümper, K. Sakai, T. Ouchi, R. Püttner, V. Sekushin, T. Tanaka, M. Hoshino, H. Tanaka, P. Decleva, K. Ueda, and F. Martín, New J. Phys. **14**, 033012 (2012).